MODELING OF DIELECTRIC FLUID SOLIDIFICATION WITH CHARGED PARTICLES IN ELECTRIC FIELDS AND REDUCED GRAVITY

George S. Dulikravich, Vineet Ahuja, and Seungsoo Lee
Department of Aerospace Engineering, The Pennsylvania State University, University Park, Pennsylvania, USA

A mathematical model and an explicit finite-difference iterative integration algorithm for two-dimensional laminar steady flow and solidification of an incompressible, viscous, electrically conducting but neutrally charged melt containing electrically charged particles and exposed to an externally applied electrostatic field were developed. The system of governing electrohydrodynamic equations was derived from a combination of Maxwell's equations and the Navier-Stokes equations, including thermally induced buoyancy, latent heat release, and Joule heating, while accounting for the mushy region. Physical properties were treated as arbitrarily temperature-dependent. Numerical results demonstrate the existence of strong electrothermoconvective motion in the melt and quantify its influence on the amount of accrued solid, deposition pattern of the electrically charged particles inside the accrued solid, and the melt/solid interface shape.

Fluid flow under the influence of a combined electromagnetic field [1] can be described by either of the two extreme models: electrohydrodynamics (EHD) or magnetohydrodynamics (MHD). The EHD model assumes a quasi-static electric field applied to a fluid containing electrically charged particles and having negligible magnetic induction effects [2–4]. The phenomenon of electrohydrodynamic instability or the generation of vorticity resulting from a nonuniform electric charge distribution in the fluid under the influence of an electric field is well known [1]. This is due to the existence of the Coulomb forces [5] that arise from the interaction of the charges and the electric potential energy.

A number of experimental observations and several simplified analytical studies have been performed on the general topic of interaction of electroconvection and heat transfer. A comprehensive review of the operational principles of the EHD in single-phase and condensation heat exchangers is provided by [6]. The injection of charges between two electrodes was dealt with in detail by Zahn and Chatelon [7]. The EHD enhancement of heat transfer has been demonstrated for

Received 2 August 1993; accepted 2 October 1993.

Computing time was provided by NASA Lewis Research Center for remotely accessing Cray C-90 computer at NAS-NASA Ames Research Center. Postprocessing was performed on equipment donated by Apple Computer, Inc.

Seungsoo Lee initiated this effort while a postdoctoral fellow at The Pennsylvania State University in 1990.

Address correspondence to George S. Dulikravich, Department of Aerospace Engineering, The Pennsylvania State University, 233 Hammond Building, University Park, PA 16802.

Numerical Heat Transfer, Part B, 25:357–373, 1994

1040–7790/94 $10.00 + .00

NOMENCLATURE

b	charged particle mobility coefficient, $m^2\,s^{-1}\,V^{-1}$	ϵ	electric permittivity coefficient, $kg\,m\,s^{-2}\,V^{-2}$
c	specific heat coefficient, $m^2\,K^{-1}\,s^{-2}$	θ	nondimensional temperature difference
D	charged particle diffusivity coefficient, $m^2\,s^{-1}$	μ	dynamic viscosity coefficient, $kg\,m^{-1}\,s^{-1}$
$\mathbf{D}^*$, $\mathbf{D}_{NS}$	diagonal matrices	ρ	fluid density, $kg\,m^{-3}$
$\mathbf{E} = \mathbf{E}(E_x, E_y)$	electric field vector, $V\,m^{-1}$	ϕ	gravity potential, $m^{-2}\,s^{-2}$
$\mathbf{g} = \mathbf{g}(g_x, g_y)$	gravity acceleration vector, $m\,s^{-2}$	φ	electric potential, V
$\mathbf{I}$	identity matrix		
k	heat conductivity coefficient, $kg\,m\,s^{-3}\,K^{-1}$	**Superscripts**	
k_B	Boltzmann constant, $kg^{-1}\,s\,K$	*	nondimensional quantity
l	length, m	′	function of nondimensional temperature
L	latent heat of solidification, $J\,kg^{-1}$	T	transpose of a matrix or a vector
p	fluid pressure, $N\,m^{-2}$		
q	electric charge/volume, $kg\,m^{-1}\,s^{-2}\,V^{-1}$	**Subscripts**	
t	time, s	cold	cold wall
T	temperature, K	E	electrical
$\mathbf{v} = \mathbf{v}(u, v)$	velocity vector in Cartesian coordinates, $m\,s^{-1}$	hot	hot wall
		l	liquid
x, y	Cartesian coordinates, m	liquidus	liquidus
α	thermal expansion coefficient, K^{-1}	s	solid
		solidus	solidus
β	artificial compressibility coefficient	0	reference values
		,	differentiation

flows between parallel plates [8] and for EHD duct flows [9]. Several simplified models of EHD liquid flows without solidification have been solved numerically in the past [10–13]. The extreme complexity of the physical phenomena and the corresponding mathematical models for the EHD [4, 12, 14, 15] seem to be the main reason for the apparent nonexistence of published research on analytical, numerical, or even experimental efforts in EHD solidification. On the other hand, several recent publications addressed analytical modeling and numerical simulation of MHD solidification under the influence of reduced gravity [15–17].

This article represents a more thorough and precise analytical model of EHD solidification/melting than our earlier work [15]. Specifically, here we elaborate on a single set of partial differential equations describing the entire phenomenon, not only in the all-melt regions, but also in the mushy (mixed melt and solid) regions, as well as in the all-solid regions. This is possible by modeling the solid phase as being yet another liquid having all the physical properties of the actual solid, except for its viscosity, which will be treated as extremely high but finite. In such a way, the actual solid-phase regions will be computationally captured as regions having practically zero internal velocity field. For the purpose of clarity, we will

often refer to the melt as "liquid" and to the extremely viscous fluid as "solid." This formulation eliminates the need to model the mushy region as a porous flow domain.

EHD SOLIDIFICATION: ANALYTICAL MODEL

The mathematical model presented in this article consists of an electrically neutral, homocompositional, viscous, incompressible liquid that is seeded with one type of charged particles having all physical properties identical to those of its immediate neighborhood media (all liquid, mushy region, or all solid) except that the particles are electrically charged. The objective is to demonstrate only fundamental effects of the applied electrostatic field, for which a single-species formulation will suffice. Although many practical solidification/melting processes involve turbulent flows, we have decided to study solidification/melting with EHD effects in laminar flows only, since reliable and universal turbulence models for EHD flows do not exist. We will also assume that there is no electrolysis or pool boiling in the liquid, and that charged particles do not undergo chaining due to their polarization (no electrorheological effects).

The system of governing equations for EHD can be derived from a combination of Maxwell's equations of electrodynamics and the Navier-Stokes equations [11–13]. An idealized charged fluid is assumed [2, 3] and, therefore, induced magnetic fields can be neglected. In the same model, the magnetic field vector and the electric polarization vector are assumed to be negligible compared to the electric field vector. Consequently, Maxwell's equations can be reduced to an electric charge conservation equation and a Poisson partial differential equation for electric potential, since the electric field is irrotational. Starting with the complete Navier-Stokes equations for compressible fluid flow and assuming that density variations as a function of temperature are small, an extended form of the Boussinesq approximation can be derived for fluids with temperature-dependent properties [11, 18]. The EHD governing equations are

$$\nabla \cdot \mathbf{v} = 0 \tag{1}$$

$$\rho \frac{D\mathbf{v}}{Dt} = -\nabla p - \rho \alpha \mathbf{g}\, \Delta T + \nabla \cdot \left\{ \mu [\nabla \mathbf{v} + (\nabla \mathbf{v})^T] \right\} + q\mathbf{E} \tag{2}$$

$$\rho c \frac{DT}{Dt} = \nabla \cdot (k \nabla T) + \mathbf{J} \cdot \mathbf{E} \tag{3}$$

$$\frac{\partial q}{\partial t} + \nabla \cdot \mathbf{J} = 0 \tag{4}$$

$$\nabla \cdot \mathbf{E} = \frac{q}{\epsilon} \tag{5}$$

Notice that the induced electric current per unit volume is given by Ohm's law,

$$\mathbf{J} = q(\mathbf{v} + b\mathbf{E}) - D \nabla q \tag{6}$$

The electric charge diffusivity coefficient, D, and charge mobility coefficient, b, are related by Einstein's formula [3, 5]:

$$D = \frac{k_B T \rho_i}{q m_i} b = 0.0025b \tag{7}$$

where m_i is the mass of a charged particle and ρ_i is the density of the electrically charged particle. Since the electric field is irrotational, it follows that

$$\mathbf{E} = -\nabla\varphi \tag{8}$$

Here, φ is the electric potential, so Eq. (5) becomes

$$\nabla^2\varphi = -\frac{q}{\epsilon} \tag{9}$$

Nondimensionalization can be performed with respect to the reference values denoted by subscript 0, so that

$$\mathbf{v}^* = \frac{\mathbf{v}}{|\mathbf{v}_0|} \qquad \mathbf{x}^* = \frac{\mathbf{x}}{l_0} \qquad t^* = \frac{t|\mathbf{v}_0|}{l_0} \qquad p^* = \frac{p}{\rho_0|\mathbf{v}_0|^2} \tag{10}$$

$$\varphi^* = \frac{\Delta\varphi}{\Delta\varphi_0} \qquad \mathbf{E}^* = \frac{\mathbf{E}l_0}{\Delta\varphi_0} \qquad q^* = \frac{q}{q_0} \qquad \theta = \frac{T - T_0}{\Delta T_0} \qquad \mathbf{g}^* = \frac{\mathbf{g}}{|\mathbf{g}_0|} \tag{11}$$

Typically, if T_{cold} is the temperature of the cold wall and T_{hot} is the temperature of the hot wall, then $\Delta T_0 = T_{\text{hot}} - T_{\text{cold}}$, where T_0 is often taken as the solidus temperature, that is, $T_0 = T_{\text{solidus}}$. Similarly, $\Delta\varphi_0$ is the reference value of the electric potential difference between the two wall electrodes. Here, for simplicity, it was assumed that the electric permittivity coefficient, ϵ, is constant.

Our objective is to use a single system of governing equations in the entire domain, which could locally contain the liquid alone, a mixture of the liquid and the solid (mushy region, where $T_{\text{liquidus}} > T > T_{\text{solidus}}$), or the solid alone. Physical properties of the liquid and the solid phases are quite different. The mass fraction of liquid at any point in the domain determines locally to what extent physical properties of the liquid or the solid phase should be taken into account. For example, latent heat released or absorbed per unit mass of the mushy region is proportional to the local volumetric ratio of liquid phase to the entire local volume. This ratio is often modeled [19] as

$$f = \frac{V_l}{V_l + V_s} = \left(\frac{\theta - \theta_{\text{solidus}}}{\theta_{\text{liquidus}} - \theta_{\text{solidus}}} \right)^n \tag{12}$$

where the exponent n is typically $0.2 < n < 5$. We will assume separate linear variations of density as a function of nondimensional temperature in the liquid and

in the solid. Thus, in the liquid we have

$$\rho_l' = 1 + \left.\frac{\partial(\rho_l/\rho_{0l})}{\partial\theta}\right|_0 (\theta - \theta_0) = 1 - \alpha_{0l}^*(\theta - \theta_0) \tag{13}$$

with a similar expression for the fluid simulating the solid phase. For certain materials, their physical properties can be significantly different in the liquid as compared to the solid phase. Density, viscosity, heat conductivity, electric charge mobility, electric charge diffusion, and heat capacity in the liquid can be expressed as arbitrary functions of nondimensional temperature:

$$\rho_l^* = \frac{\rho_{0l}}{\rho_0}\rho_l' \qquad \mu_l^* = \frac{\mu_{0l}}{\mu_0}\mu_l' \qquad k_l^* = \frac{k_{0l}}{k_0}k_l' \qquad b_l^* = \frac{b_{0l}}{b_0}b_l' \tag{14}$$

$$D_l^* = \frac{D_{0l}}{D_0}D_l' \qquad c_l^* = \frac{c_{0l}}{c_0}c_l' \qquad \alpha_l^* = \frac{\alpha_{0l}}{\alpha_0} \qquad \epsilon_l^* = \frac{\epsilon_{0l}}{\epsilon_0} \tag{15}$$

with similar expressions for the fluid simulating the solid phase. Here, we assume thermal expansion coefficients and electric permitivity coefficients to be temperature nondependent in both the liquid and the solid phase. We can now introduce nondimensional numbers defined as follows:

Reynolds number
$$\mathrm{Re} = \frac{\rho_0|\mathbf{v}_0|l_0}{\mu_0}$$

Prandtl number
$$\mathrm{Pr} = \frac{c_0\mu_0}{k_0} \tag{16}$$

Grashof number
$$\mathrm{Gr} = \frac{\rho_0^2|\mathbf{g}_0|\alpha_0\,\Delta T_0 l_0^3}{\mu_0^2}$$

Eckert number
$$\mathrm{Ec} = \frac{|\mathbf{v}_0|^2}{c_0\,\Delta T_0} \tag{17}$$

Froude number
$$\mathrm{Fr}^2 = \frac{|\mathbf{v}_0|^2}{|\mathbf{g}_0|l_0}$$

Stefan number
$$\mathrm{Ste} = \frac{c_0\,\Delta T_0}{L_0} \tag{18}$$

Charge diffusivity number
$$D_E = \frac{\mu_0}{\rho_0 D_0}$$

Coulomb force number
$$S_E = \frac{q_0\,\Delta\varphi_0}{\rho_0|\mathbf{v}_0|^2} \tag{19}$$

Electric Prandtl number
$$\mathrm{Pr}_E = \frac{\mu_0}{\rho_0 b_0\,\Delta\varphi_0}$$

Electric field number
$$N_E = \frac{q_0 l_0^2}{\epsilon_0\,\Delta\varphi_0} \tag{20}$$

The nondimensional system of equations that is valid throughout the computational domain comprising the liquid, the mushy region, and the solid with separate temperature-dependent physical properties in each phase and containing charged particles while under the influence of electrostatic and gravitational arbitrarily oriented fields expressed in a conservative form, is
Mass conservation equation

$$\nabla^* \cdot \mathbf{v}^* = 0 \tag{21}$$

Linear momentum conservation equation

$$\begin{aligned}\bar{\bar{\rho}}^* \frac{\partial \mathbf{v}^*}{\partial t^*} + f\rho_l^* \nabla^* \cdot (\mathbf{v}^*\mathbf{v}^* + \bar{\bar{p}}_l^* \mathbf{I}) + (1-f)\rho_s^* \nabla^* \cdot (\mathbf{v}^*\mathbf{v}^* + \bar{\bar{p}}_s^* \mathbf{I}) \\ = f \nabla^* \cdot \left\{ \frac{\mu_l^*}{\mathrm{Re}} [\nabla^*\mathbf{v}^* + (\nabla^*\mathbf{v}^*)^T] \right\} + \bar{\bar{\alpha}}^* \frac{\mathrm{Gr}\,\theta}{\mathrm{Re}^2} \mathbf{g}^* \\ + (1-f) \nabla^* \cdot \left\{ \frac{\mu_s^*}{\mathrm{Re}} [\nabla^*\mathbf{v}^* + (\nabla^*\mathbf{v}^*)^T] \right\} + S_E\, q^* \mathbf{E}^*\end{aligned} \tag{22}$$

Energy conservation equation

$$\begin{aligned}\bar{\bar{c}}^* \frac{\partial \theta}{\partial t^*} + f\rho_l^* \nabla^* \cdot (c_{el}^* \theta \mathbf{v}^*) + (1-f)\rho_s^* \nabla^* \cdot (c_{es}^* \theta \mathbf{v}^*) \\ = \frac{1}{\mathrm{Re}\,\mathrm{Pr}} [f \nabla^* \cdot (k_l^* \nabla^*\theta) + (1-f) \nabla^* \cdot (k_s^* \nabla^*\theta)] \\ + S_E\, \mathrm{Ec} \left(q^* \mathbf{v}^* \cdot \mathbf{E}^* + q^* \bar{\bar{b}}^* \frac{\mathbf{E}^* \cdot \mathbf{E}^*}{\mathrm{Re}\,\mathrm{Pr}_E} - \bar{\bar{b}}^* \frac{\nabla^* q^* \cdot \mathbf{E}^*}{\mathrm{Re}\, D_E} \right)\end{aligned} \tag{23}$$

Charge conservation equation

$$\frac{\partial q^*}{\partial t^*} + \nabla^* \cdot \left[q^* \left(\mathbf{v}^* + \frac{\bar{\bar{b}}^* \mathbf{E}^*}{\mathrm{Re}\,\mathrm{Pr}_E} \right) \right] = \frac{1}{\mathrm{Re}\, D_E} \nabla^* \cdot (\bar{\bar{b}}^* \nabla^* q^*) \tag{24}$$

Electric potential equation

$$\nabla^{*2} \varphi^* = -N_E q^* \left(\frac{f}{\epsilon_l^*} + \frac{(1-f)}{\epsilon_s^*} \right) \tag{25}$$

Here, we used the following symbols for the mixture density, mobility, heat capacity, and thermal expansion:

$$\bar{\bar{p}}^* = f\rho_l^* + (1-f)\rho_s^* \tag{26}$$

$$\bar{\bar{b}}^* = fb_l^* + (1-f)b_s^* \tag{27}$$

$$\bar{\bar{c}}^* = f\rho_l^* \frac{\partial (c_{le}^* \theta)}{\partial \theta^*} + (1-f)\rho_s^* \frac{\partial (c_{se}^* \theta)}{\partial \theta^*} \tag{28}$$

$$\bar{\bar{\alpha}}^* = f\rho_l^* \alpha_l^* + (1-f)\rho_s^* \alpha_s^* \tag{29}$$

Combination of hydrodynamic and hydrostatic pressures,

$$\bar{\bar{p}}_l^* = \frac{p^*}{\rho_l^*} + \frac{\phi^*}{\mathrm{Fr}^2} \quad \text{and} \quad \bar{\bar{p}}_s^* = \frac{p^*}{\rho_s^*} + \frac{\phi^*}{\mathrm{Fr}^2} \tag{30}$$

uses the nondimensional gravity potential ϕ^*, defined as $\mathbf{g}^* = \nabla^*\phi^*$. We used an enthalpy method to formulate the equivalent specific heat coefficient in the liquid and the solid phases as

$$c_{le}^* = c_l^* - \frac{1}{\mathrm{Ste}} \frac{\partial f}{\partial \theta} \quad \text{and} \quad c_{se}^* = c_s^* - \frac{1}{\mathrm{Ste}} \frac{\partial f}{\partial \theta}$$

respectively. This expression allows for the latent heat to be released in the mushy region according to the empirical law (12). Viscous dissipation can be neglected [11, 18], since its ratio with respect to the convective term in the energy equation is of the order Ec/Re, which is typically a small number in natural convection.

EHD SOLIDIFICATION: NUMERICAL MODEL

For the purpose of developing a versatile EHD solidification/melting analysis code applicable to arbitrary configurations where correct boundary conditions could be easily enforced precisely at the boundaries, the system of equations (21)–(24) was transformed into a fully conservative vector form expressed in general curvilinear, boundary-conforming, nonorthogonal coordinates (ξ, η) [11–13] as

$$\begin{aligned}
&\mathbf{D}^* \frac{\partial \tilde{\mathbf{Q}}^*}{\partial t^*} + f\left(\frac{\partial \tilde{\mathbf{E}}^{l*}}{\partial \xi^*} + \frac{\partial \tilde{\mathbf{F}}^{l*}}{\partial \eta^*}\right) + (1-f)\left(\frac{\partial \tilde{\mathbf{E}}^{s*}}{\partial \xi^*} + \frac{\partial \tilde{\mathbf{F}}^{s}}{\partial \eta^*}\right) \\
&\quad = \mathbf{D}_{\mathrm{NS}}\left\{ f\left[\frac{\partial}{\partial \xi^*}\left(\frac{\mathbf{D}_{\mathrm{NS}}^{*l}}{J} g_{ij} \frac{\partial J\tilde{\mathbf{Q}}^*}{\partial \xi^*}\right) + \frac{\partial}{\partial \eta^*}\left(\frac{\mathbf{D}_{\mathrm{NS}}^{*l}}{J} g_{ij} \frac{\partial J\tilde{\mathbf{Q}}^*}{\partial \eta^*}\right)\right] + \mathbf{S}^* \right. \\
&\qquad \left. + (1-f)\left[\frac{\partial}{\partial \xi^*}\left(\frac{\mathbf{D}_{\mathrm{NS}}^{*s}}{J} g_{ij} \frac{\partial J\tilde{\mathbf{Q}}^*}{\partial \xi^*}\right) + \frac{\partial}{\partial \eta^*}\left(\frac{\mathbf{D}_{\mathrm{NS}}^{*s}}{J} g_{ij} \frac{\partial J\tilde{\mathbf{Q}}^*}{\partial \eta^*}\right)\right]\right\}
\end{aligned} \tag{31}$$

where the solution vector $\mathbf{Q}^*$ and the general flux vectors $\mathbf{E}^{*l}$ and $\mathbf{F}^{*l}$ are

$$\tilde{\mathbf{Q}}^* = \frac{1}{J}\left\{\frac{p^*}{\beta}\ u^*\ v^*\ \theta\ q^*\right\}^T \tag{32}$$

$$\tilde{\mathbf{E}}^{l*} = \frac{1}{J}\begin{Bmatrix} U^* \\ U^*u^* + \xi_{,x}\bar{\bar{p}}_l^* \\ U^*v^* + \xi_{,y}\bar{\bar{p}}_l^* \\ U^*\theta \\ \theta\left(U^* + \dfrac{b_l^* E_\xi^*}{\mathrm{Re}\,\mathrm{Pr}_E}\right) \end{Bmatrix} \qquad \tilde{\mathbf{F}}^{l*} = \frac{1}{J}\begin{Bmatrix} V^* \\ V^*u^* + \eta_{,x}\bar{\bar{p}}_l^* \\ V^*v^* + \eta_{,y}\bar{\bar{p}}_l^* \\ V^*\theta \\ \theta\left(V^* + \dfrac{b_l^* E_\eta^*}{\mathrm{Re}\,\mathrm{Pr}_E}\right) \end{Bmatrix} \tag{33}$$

with similar expressions for the flux vectors $\tilde{\mathbf{E}}^{s*}$ and $\tilde{\mathbf{F}}^{s*}$. The source vector is

$$\mathbf{S}^* = \begin{Bmatrix} 0 \\ \bar{\bar{\alpha}}^* \dfrac{\mathrm{Gr}\,\theta}{\mathrm{Re}^2} g_x^* + S_E q^* \mathbf{E}_x^* \\ \bar{\bar{\alpha}}^* \dfrac{\mathrm{Gr}\,\theta}{\mathrm{Re}^2} g_y^* + S_E q^* \mathbf{E}_y \\ S_E\,\mathrm{Ec}\left[q^*\left(\mathbf{v}^* \cdot \mathbf{E}^* + \bar{\bar{b}}^* \dfrac{\mathbf{E}^* \cdot \mathbf{E}^*}{\mathrm{Re}\,\mathrm{Pr}_E}\right) - \bar{\bar{b}}^* \dfrac{\nabla^* q^* \cdot \mathbf{E}^*}{\mathrm{Re}\,D_E}\right] \end{Bmatrix} \tag{34}$$

Here, diagonal coefficient matrices are

$$\mathbf{D}^* = \mathrm{diag}\left[1\,\bar{\bar{\rho}}\bar{\bar{\rho}}\bar{\bar{c}}1\right]$$

$$\mathbf{D}_{\mathrm{NS}} = \mathrm{diag}\left[0\,\frac{1}{\mathrm{Re}}\,\frac{1}{\mathrm{Re}}\,\frac{1}{\mathrm{Re}\,\mathrm{Pr}}\,\frac{1}{\mathrm{Re}\,D_E}\right] \tag{35}$$

$$\mathbf{D}_{\mathrm{NS}}^{*l} = \mathrm{diag}[0\,\mu_l^*\,\mu_l^*\,k_l^*\,b_l^*] \qquad \mathbf{D}_{\mathrm{NS}}^{*s} = \mathrm{diag}[0\,\mu_s^*\,\mu_s^*\,k_s^*\,b_s^*] \tag{36}$$

Here, $J = \det[\partial(\xi, \eta)/\partial(x, y)]$ and g_{ij} is the metric tensor given by $g_{ij} = \nabla x_i' \nabla x_j'$, while U^* and V^* are the nondimensionalized contravariant velocity vector components. A nonphysical artificial [20] compressibility term, $\partial(p^*/\beta)/\partial t^*$, was added so that the system (31) can be made nonsingular and integrated in time simultaneously. The parameter β is a constant specified by the user. The system of coupled nonlinear partial differential equations (31) was discretized using central differencing and integrated iteratively using a four-stage explicit Runge-Kutta time stepping [21] given as

$$\left.\begin{aligned} \tilde{\mathbf{Q}}^0 &= \mathbf{Q}^n \\ \Delta\tilde{\mathbf{Q}}^m &= -\gamma_m\,\Delta t^*\,\tilde{\mathbf{R}}^{m-1} \\ \tilde{\mathbf{Q}}^{n+1} &= \tilde{\mathbf{Q}}^n + \Delta\tilde{\mathbf{Q}}^4 \end{aligned}\right\} \qquad m = 1, 2, 3, 4 \tag{37}$$

where the iteration level is denoted by n, and each stage of the Runge-Kutta algorithm is denoted by m. Here the coefficients are $\gamma_m = 1/4$, $1/3$, $1/2$, and 1,

respectively. The residual vector $\tilde{\mathbf{R}}$ is computed by moving all terms from the right side of the system (31) to its left side and explicitly adding a small amount of fourth-order artificial dissipation to stabilize the algorithm, which is otherwise prone to oscillations due to even–odd decoupling because it uses central differencing in space. Poisson's equation (25) for electric potential was solved separately during each global iteration using a fast, alternating-direction, implicit algorithm. Wall pressures were computed from the normal momentum equation. Boundary conditions for electric charges on the electrically isolated boundaries were of the Neumann type. Otherwise, electric charges were injected uniformly at one boundary and their pattern was computed at the opposite boundary.

NUMERICAL RESULTS

Based on our theoretical model and the numerical algorithm, a FORTRAN code was developed that is capable of predicting details of the convection and conduction heat transfer in EHD flows involving solidification/melting. We are not aware of any publications dealing with EHD solidification of dielectric fluids. Consequently, we chose a sequence of simple test cases to demonstrate the ability to simulate this phenomenon without having an opportunity to thoroughly verify the accuracy of our analytical model and the numerical algorithm against published experimental or computational data. Although the code is applicable to arbitrary two-dimensional configurations, for the purpose of analyzing the fundamental phenomena we chose to test solidification processes numerically in a simple configuration consisting of a closed, horizontal, two-dimensional rectangular container of aspect ratio 2:1 ($l_0 = 0.033333$ m in height), fully filled with the molten gallium arsenide. The container area was discretized with a symmetrically clustered orthogonal computational grid having 60×60 rectangular grid cells. Physical properties used in this work are summarized in Table 1, and the corresponding nondimensional numbers are given in Table 2. Since we did not have reliable information as to the typical level of the electric charges and mobilities, we used $q_0 = 1 \times 10^{-4}$ C m^{-3} and $b_0 = 1 \times 10^{-8}$ m^2 V^{-1} s^{-1} as the reference values, which correspond to an aqueous biological solution [22]. Since there is no mean velocity in this type of flow, we defined the Reynolds number as $\mathrm{Re} = \mathrm{Gr}^{1/2}$, which determines the reference velocity in full gravity as $v_0 = 0.02473$ m s^{-1} and in reduced gravity test cases as $v_0 = 0.002473$ m s^{-1}. All other reference values used in the nondimensionalization corresponded to the liquidus temperature (Table 1). The following nondimensional numbers were used in all the test cases: $\mathrm{Pr} = 0.068$, $\mathrm{Ste} = 5.98 \times 10^{-3}$, $D_E = 1.95 \times 10^{-4}$. The top wall was specified as uniformly cold at $\theta = -0.5$ ($T_{\mathrm{cold}} = 1506.005$ K), the bottom wall was uniformly hot at $\theta = 0.5$ ($T_{\mathrm{hot}} = 1516.005$ K), while vertical walls were adiabatic. The gravity vector was applied vertically downward. Initial guesses were $\mathbf{v} = 0$, $p = 0$, $\theta = 0.5$, $q = q_0$ (or $q = 0$), and $\mathbf{E} =$ constant (or $\mathbf{E} = 0$). Several distinct test cases were analyzed numerically.

Case 1. There was no electric field applied in this case, and no charged particles were introduced while full gravity force was applied ($\mathbf{g}^* = 1.0$). This is the typical case of solidification from above, where two strong thermoconvective, counterrotating vortices (Figure 1*a*) exist in the steady-state situation below the

Table 1. Physical Properties of GaAs

Symbols and units	Value	Reference
ρ_l [kg m^{-3}]	5710.0	23
ρ_s [kg m^{-3}]	5196.0	24, p. 1.1
c_l [J kg^{-1} K^{-1}]	434.0	23
c_s [J kg^{-1} K^{-1}]	416.0	24, p. 1.8
k_l [W m^{-1} K^{-1}]	17.8	23
k_s [W m^{-1} K^{-1}]	7.0	23
T_l [K]	1511.005	Assumed
T_s [K]	1511.0	23
b_l [m^2 V^{-1}]	1×10^{-8}	22
b_s [m^2 V^{-1}]	1×10^{-14}	Assumed
D_l [m^2 s^{-1}]	2.5×10^{-10}	5
D_s [m^2 s^{-1}]	2.5×10^{-16}	5
α_l [K^{-1}]	1.87×10^{-4}	23
α_s [K^{-1}]	5.0×10^{-4}	16
σ_l [W^{-1} m^{-1}]	8.0×10^{5}	23
σ_s [W^{-1} m^{-1}]	3.0×10^{4}	23
ϵ_l	708×10^{-12}	22
ϵ_s	1×10^{-12}	Assumed
μ [kg m^{-1} s^{-1}]	$2.79 - 0.005\,(T - 1511) \times 10^{-3}$	23, 25
L [J kg^{-1}]	726,000	23

solid that accrued on the top wall. Strong temperature gradients exist inside the solid, and the solid/liquid interface is highly curved (Figure 1*b*). Due to the strong convection in this test case, the computed normal temperature gradients (negative) at the bottom wall and at the top wall are highly nonuniform (Figure 1*c*). Notice that differences in the magnitudes of the arrows in Figure 1*c* at the top and bottom walls are due to the fact that the thermal conductivities of liquid and solid GaAs are quite different (Table 1). The predicted solidified volume was 10.96% of the total container volume (Table 2). When running this same test case with 1% of

Table 2. Input Parameters for EHD Solidification of GaAs Melt in a 2:1-Aspect-Ratio Closed Container[a]

	Case no. 1	Case no. 2	Case no. 3	Case no. 4	Case no. 5
g	1	1	0.01	1	0.01
$\Delta\varphi(V)$	0	5000 ↑	1000 ↑	15000 →	1000 →
Re	1687	1687	168.7	1687	168.7
Gr	2.85×10^{6}	2.85×10^{6}	2.85×10^{4}	2.85×10^{6}	2.85×10^{4}
Ec	1.41×10^{-7}	1.41×10^{-7}	1.41×10^{-9}	1.41×10^{-7}	1.41×10^{-9}
N_E	NA	0.222	0.222	0.07407	0.111
S_E	NA	0.143	14.3	0.429	28.6
Pr_E	NA	9.77×10^{-3}	9.77×10^{-3}	3.26×10^{-3}	4.88×10^{-3}
Solid(%)	10.96	10.82	27.48	10.88	28.30

[a]Arrows designate orientation of the uniform electrostatic field vector **E**.

terrestrial gravity ($\mathbf{g}^* = 0.01$), only mild convection started initially. Nevertheless, as the solidification front advanced downward from the top wall, the effective melt height reduced, thus strongly reducing the Grashof number and the effective Rayleigh number ($\mathrm{Ra} = \mathrm{Gr}\,\mathrm{Pr}$). Consequently, the effective Rayleigh number became subcritical and thermal convection ceased altogether. As a result, this test case produced a steady state with pure conduction in the accrued solid and in the melt below. The predicted isotherms were practically horizontal, and the predicted solidified volume was 29.17% of the total container volume.

Case 2. A uniform external electrostatic field of 5000 V was applied in this case acting upward, as was the full gravity force ($\mathbf{g}^* = 1.0$). We enforced uniform charged particle concentration at the lower wall while treating the top wall as an exit boundary for the charged particles, since the side walls had a Neumann condition imposed on electric charges. Negligible differences between the results in

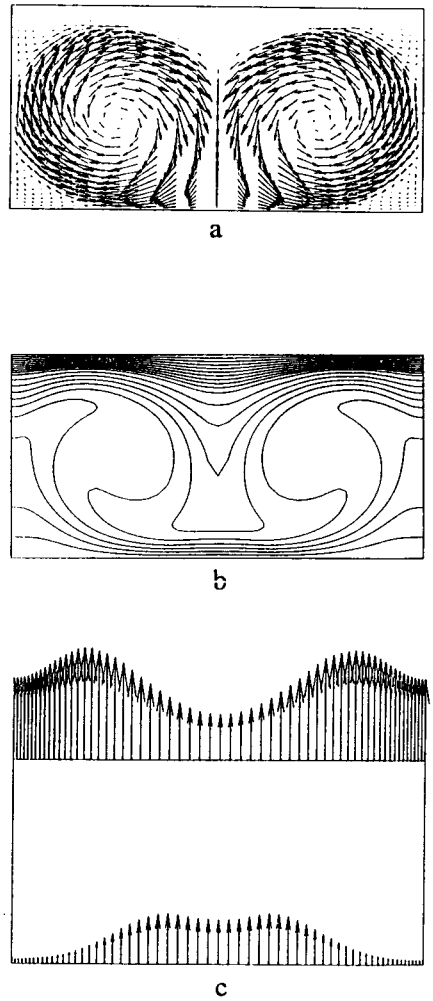

Figure 1. Case 1—solid accrues from top wall. Full gravity without electric field and charged particles: (**a**) velocity vector field due to thermoconvection; (**b**) isotherms in the accrued solid and in the melt; (**c**) normal temperature derivatives (negative) on the top and the bottom walls.

this case and in the previous case have been observed. The computed velocity field (Figure 2*a*), temperature field (Figure 2*b*), and the normal derivatives (negative) of temperature at the top and the bottom walls (Figure 2*c*) were practically the same as in Figures 1*a*, 1*b*, and 1*c*. Consequently, an almost identical amount of accrued solid (10.82% of the container volume) was predicted. Thus, a stronger electric field is needed in full gravity to influence the strong thermal convection.

Case 3. A uniform external electrostatic field of 1000 V was applied in this case acting upward, as was a low normalized gravity force ($\mathbf{g}^* = 0.01$). We enforced a uniform distribution of the charged particles at the lower wall while treating the top wall as an exit boundary for the charged particles, since the side walls had a Neumann condition imposed on electric charges. The resulting Coulomb force in this case was strong enough to overcome the viscous force and cause a pure electroconvection (Figure 3*a*) consisting of two weak, counterrotating vortices. The

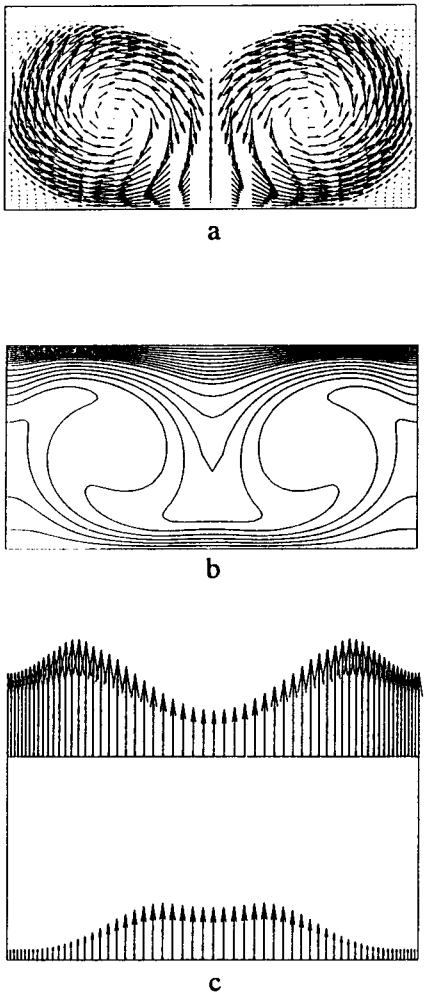

Figure 2. Case 2—solid accrues from top wall. Full gravity with $\Delta\varphi = 5000$ V electric field acting vertically upward and charged particles: (**a**) velocity vector field due to combined electrothermoconvection; (**b**) isotherms in the accrued solid and in the melt; (**c**) normal temperature derivatives (negative) on the top and the bottom walls.

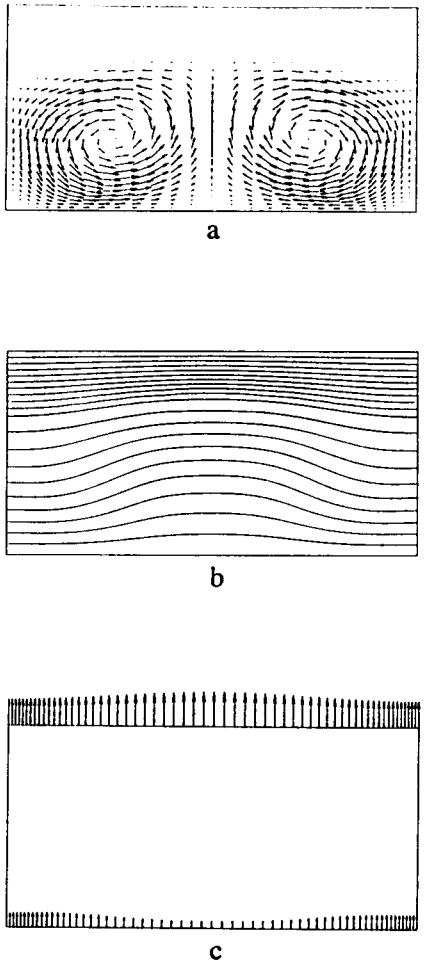

Figure 3. Case 3—solid accrues from top wall. Reduced gravity with $\Delta\varphi = 1000$ V electric field acting vertically upward and charged particles: (**a**) velocity vector field due to combined electrothermoconvection; (**b**) isotherms in the accrued solid and in the melt; (**c**) normal temperature derivatives (negative) on the top and the bottom walls.

predicted isotherms (Figure 3*b*) are mildly curved, while the predicted normal temperature derivatives at the top and the bottom walls (Figure 3*c*) are only mildly nonuniform. Predicted volume of the accrued solid in this case was 27.48% of the total volume of the container.

Case 4. In this case an external electrostatic field of 15,000 V was applied horizontally while full gravity ($\mathbf{g}^* = 1.0$) acted vertically downward. A uniform electric charge density was specified at the left vertical wall, normal derivatives of charges were zero at the top and the bottom walls, and charges were computed at the right vertical wall. Because of the strong interaction of thermal buoyancy and the electroconvection, this case resulted in a highly asymmetric solution containing a complex pattern of counterrotating vortices (Figure 4*a*). The asymmetry is obvious in the predicted thermal field (Figure 4*b*) and the corresponding normal temperature derivatives at the top and the bottom walls (Figure 4*c*). This test case resulted in 10.88% of the total volume solidified.

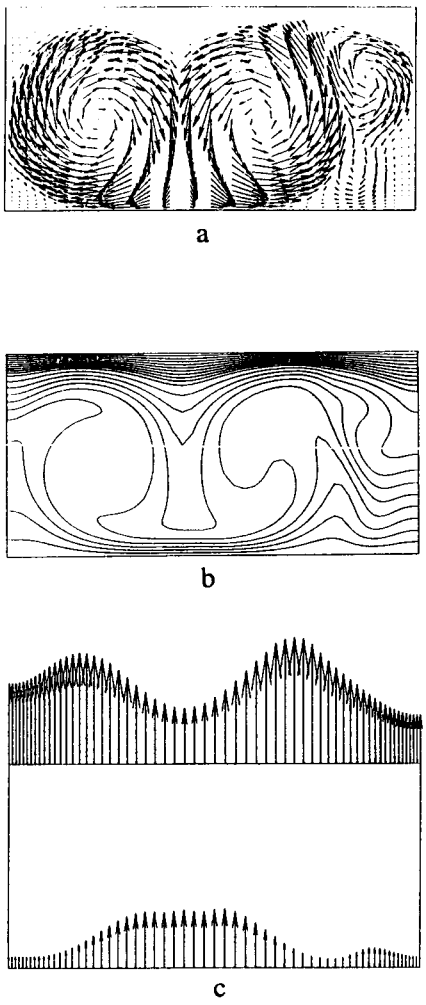

Figure 4. Case 4—solid accrues from top wall. Full gravity with $\Delta\varphi = 15{,}000$ V electric field acting horizontally from left to right and charged particles: (**a**) velocity vector field due to combined electrothermoconvection; (**b**) isotherms in the accrued solid and in the melt; (**c**) normal temperature derivatives (negative) on the top and the bottom walls.

Case 5. In this case an external electrostatic field of 1000 V was applied horizontally while reduced gravity ($g^* = 0.01$) acted vertically downward. The electric charges were specified as uniform at the left vertical wall. A dramatic change of pattern of the resulting electroconvection lead to a single asymmetric vortex (Figure 5*a*), causing also a slight asymmetry in the predicted isotherms (Figure 5*b*) and the normal temperature derivatives at the bottom and the top walls (Figure 5*c*). This time the predicted solidified volume was 27% of the container volume.

In order to demonstrate the insensitivity of the computer code to grid refinement, we ran the first test case on 120×120 symmetrically clustered grid cells. The resulting melt flow pattern was practically indistinguishable from the pattern obtained with the grid consisting of 60×60 grid cells. In addition, the

amount of solid accrued on the refined grid differed by less than half of one percent from the amount of solid accrued on the coarser grid.

CONCLUSIONS

A complex analytical model capable of simultaneously capturing thermoconvective and electroconvective motion inside a liquid, details of the mushy region, and the accrued solid phase have been successfully implemented numerically for the cases with electrically charged particles and arbitrary externally applied electrostatic and gravitational fields. Numerical simulation of two-dimensional solidification from above a GaAs melt reveals that the electrostatic field has definite consequences on the thermal field inside the melt and the solid accrued because of the creation of electroconvection. Consequently, predicted wall heat fluxes with the applied electrostatic field differ significantly from those without the electric field

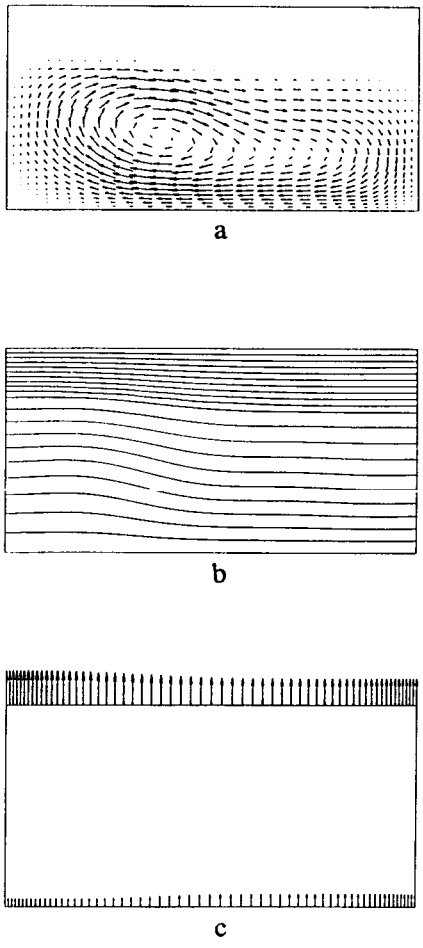

Figure 5. Case 5—solid accrues from top wall. Reduced gravity with $\Delta\varphi = 1000$ V electric field acting horizontally from left to right and charged particles: (**a**) velocity vector field due to combined electrothermoconvection; (**b**) isotherms in the accrued solid and in the melt; (**c**) normal temperature derivatives (negative) on the top and the bottom walls.

applied. These effects are more pronounced in the reduced gravity environment than in the full gravity environment for low Rayleigh numbers. Computational results indicate the extreme importance of understanding the interplay between the externally imposed electric and gravitational field strengths and orientations. If the solidification process had been simulated with a time-accurate code, precise impurities deposition pattern inside the solid could be predicted. This suggests possibilities to develop an algorithm for a judicious application of the external electric field to actively control impurities or dopant deposition pattern in the crystal, heat transfer at the boundaries, the amount of solid accrued, and the solid/liquid interface shape.

REFERENCES

1. L. D. Landau and E. M. Lifshitz, *Electrodynamics of Continuous Media*, Pergamon Press, New York, 1960.
2. O. M. Stuetzer, Magnetohydrodynamics and Electrohydrodynamics, *Phys. Fluids*, vol. 5, no. 5, pp. 534–544, 1962.
3. J. R. Melcher, *Continuum Electromechanics*, MIT Press, Cambridge, Mass., 1981.
4. V. G. Babskii, M. Y. Zhukov, and V. I. Yudovich, *Mathematical Theory of Electrophoresis* (translated by C. Flick), Consultants Bureau, New York, 1989.
5. A. C. Eringen and G. A. Maugin, *Electrodynamics of Continua II; Fluids and Complex Media*, Springer-Verlag, New York, pp. 562–563, 1990.
6. M. M. Ohadi, Heat Transfer Enhancement in Heat Exchangers, *ASHRAE J.*, vol. 33, no. 12, pp. 42–50, 1991.
7. M. Zahn and H. Chatelon, Charge Injection between Concentric Cylindrical Electrodes, *J. Appl. Phys.*, vol. 48, no. 5, pp. 1797–1805, 1977.
8. T. Fujino, Y. Yokoyama, and Y. H. Mori, Augmentation of Laminar Forced Convection Heat Transfer by Application of a Transverse Electric Field, *J. Heat Transfer*, vol. 111, pp. 345–351, 1989.
9. J. L. Fernandez and R. Poulter, Radial Mass Flow in Electrohydrodynamically-Enhanced Forced Heat Transfer in Tubes, *Int. J. Heat Mass Transfer*, vol. 30, no. 10, pp. 2125–2136, 1987.
10. M. S. Bello and V. I. Polezhaev, Hydrodynamics, Gravitational Sensitivity and Transport Phenomena in Continuous Flow Electrophoresis, AIAA Paper 91-0112, Aerospace Sciences Meeting, Reno, Nev., Jan. 7–10, 1991.
11. S. Lee, G. S. Dulikravich, and B. Kosovic, Electrohydrodynamic (EHD) Flow Modeling and Computations, AIAA Paper 91-1469, AIAA Fluid, Plasma Dynamics and Lasers Conf., Honolulu, Hawaii, June 24–26, 1991.
12. G. S. Dulikravich, V. Ahuja, and S. Lee, Computation of Electro-Thermo-Convective Phenomena in Electro-Rheological Fluids, ASME Fluids Engineering Summer Meeting, in D. A. Siginer, J. H. Kim, and R. A. Bajura (eds.), Proc. of Symposium on Electro-Rheological Flows, Washington, D.C., June 21–24, 1993, ASME FED-Vol. 164, pp. 29–42, 1993a.
13. G. S. Dulikravich, V. Ahuja, and S. Lee, Simulation of Electrohydrodynamic Enhancement of Laminar Flow Heat Transfer, ASME National Heat Transfer Conf., Atlanta, Ga., Aug. 8–11, 1993, in Y. Bayazitoglu and V. S. Arpaci (eds.), Proc. Symp. on Fundamentals of Heat Transfer in Electromagnetic, Electrostatic, and Acoustic Fields, ASME HTD-Vol. 248, pp. 43–52; also in *J. Enhanced Heat Transfer*, vol. 1, no. 1, Aug. 1993b.

14. A. Hosseini-Sianaki, R. Firoozian, D. J. Peel, and W. A. Bullough, Comparative Methods for the Derivation of In Flow Electrical Characteristics of Electro-Rheological Fluids, *J. Intelligent Material Systems and Structures*, vol. 3, pp. 96–111, 1992.
15. G. S. Dulikravich and B. Kosovic, Solidification of Variable Property Melts under the Influence of Low Gravity, Magnetic Fields and Electric Fields, AIAA Paper 92-0694, AIAA Aerospace Sciences Meeting, Reno, Nev., Jan. 6–9, 1992.
16. S. Motakeff, Magnetic Field Elimination of Convective Interference with Segregation during Vertical-Bridgman Growth of Doped Semiconductors, *J. Crystal Growth*, vol. 104, pp. 833–850, 1990.
17. G. S. Dulikravich, V. Ahuja, and S. Lee, Three-Dimensional Solidification with Magnetic Fields and Reduced Gravity, AIAA Paper 93-0912, Reno, Nev., Jan. 11–14, 1993; also to appear in *Int. J. Heat Mass Transfer*, 1994.
18. D. D. Gray and A. Giorgini, The Validity of the Bousinessq Approximation for Liquids and Gases, *Int. J. Heat Mass Transfer*, vol. 19, pp. 545–551, 1976.
19. V. R. Voller and C. R. Swaminathan, General Source-Based Method for Solidification Phase Change, *Numer. Heat Transfer, Part B*, vol. 19, pp. 175–189, 1991.
20. A. J. Chorin, A Numerical Method for Solving Incompressible Viscous Flow Problems, *J. Comput. Phys.*, vol. 2, pp. 12–26, 1967.
21. A. Jameson, W. Schmidt, and E. Turkel, Numerical Solutions of the Euler Equations by Finite Volume Methods Using Runge-Kutta Time-Stepping Scheme, AIAA Paper 81-1259, Palo Alto, Calif., June 1981.
22. D. A. Saville and O. A. Palusinski, Theory of Electrophoretic Separations, *AIChE J.*, vol. 32, no. 2, pp. 207–214, 1986.
23. P. Sabhapathy and M. E. Salcudean, Numerical Study of Flow and Heat Transfer in LEC Growth of GaAs With an Axial Magnetic Field, *J. Crystal Growth*, vol. 104, pp. 371–388, 1990.
24. M. H. Brodsky, *Properties of Gallium Arsenide*, 2d ed., INSPEC, EMIS Datareview Series No. 2, 1990.
25. M. J. Crochet, F. T. Geyling, and J. J. Van Schaftingen, Numerical Simulation of the Horizontal Bridgman Growth. Part I: Two-Dimensional Flow, *Int. J. Numer. Meth. Fluids*, vol. 7, pp. 29–47, 1987.